

Energetic benefits in coordinated circular swimming motion of two swimmersDanshi Liu, Jiadong Wang, Xuewei Mao, and Jian Deng ^{*}*Department of Mechanics, Zhejiang University, Hangzhou 310027, People's Republic of China*

(Received 12 March 2023; accepted 13 September 2023; published 9 November 2023)

The coordinated movement of multiple swimmers is a crucial component of fish schools. Fish swimming in different formations, such as tandem, side-by-side, diamond, and phalanx, can achieve significant energetic advantages. However, the energetic benefits of nonstraight swimming behaviors, such as the collective motion of a milling pattern, are not well understood. To fill in this gap, we consider two swimmers in circular tracks, controlled by a PID approach to reach stable configurations. Our study finds that the optimal phase is affected by circumferential effects, and that substantial energy savings can result from both propulsion and turning. We also explore the radial effect in terms of energetic benefits. In a milling pattern, the inner swimmers can easily gain a certain energetic benefit (−8%), while their peers on the outside must be close enough to the inner swimmer with a proper phase to gain the energetic benefit (−14%). When the radial spacing becomes larger or is in an unmatched phase, the swimming of the outer swimmers becomes more laborious (+16%). Our results indicate that swimmers who maintain a matched phase and minimum radial effect obtain the highest energetic benefits (−26%). These findings highlight the energetic benefits of swimmers, even in a milling pattern, where the position difference dominates the extent of benefit.

DOI: [10.1103/PhysRevE.108.054603](https://doi.org/10.1103/PhysRevE.108.054603)**I. INTRODUCTION**

Collective behavior is a prevalent phenomenon in nature, observed in diverse animal groups such as army ant colonies, zebra herds, starling flocks, and schools of sardines. It is believed that coordinated motion among individuals offers several advantages, ranging from collective escape [1–4] to enhanced exploration capabilities for foraging [5–8]. Fish schools, in particular, have been found to serve various biological functions, including reducing predation risk [9–11], increasing feeding and reproductive opportunities [6], and decreasing energy expenditure [12]. From a fluid dynamics perspective, it is suggested that the collective behavior of fish provides hydrodynamic benefits. The flow-mediated interaction is a crucial factor in fish swimming, and those employing body undulation as their primary means of propulsion exhibit superior propulsive efficiency and maneuverability compared to most engineered vehicles [13,14].

Early investigations of fish swimming behavior were primarily conducted through theoretical analysis and experimental measurements [6,7,12,15–19]. With the advancement in computational power, computational fluid dynamics (CFD) has emerged as a promising approach to study fish swimming in recent years [20–31]. Numerous studies have focused on optimizing fish shape or swimming motion, as well as on how one fish may exploit the vortical structures generated by the unsteady motions of another swimming fish to save energy. Indeed, it has been demonstrated that a fish can leverage vortices to reduce locomotion cost [32]. Moreover, experiments investigating swimming behaviors of fish groups have revealed a

reduction in energy expenditure based on respirometer readings and reduced tail-beat frequency. Fishes are capable of sensing and navigating in complex flow fields characterized by mechanical energy distributed across multiple scales due to vortices generated by obstacles, peers, and other swimming organisms.

In the study of fish schooling, both experimental and numerical methods have been employed to investigate collective behavior [33–37], with a particular focus on the remarkable energy benefits associated with different configurations. Simple schooling models, including tandem and side-by-side arrangements, have been extensively explored. Notably, previous research has unequivocally demonstrated the profound influence of formation dynamics on energy efficiency. In tandem formations, the downstream body experiences significant wake interactions caused by the shedding vortices of the leader, altering the oncoming flow and the effective angle of attack for the follower [33,38,39]. Side-by-side formations have revealed that antiphase flapping motion enhances thrust and cruising speed, while in-phase flapping conserves power [40–45]. Furthermore, the energy-saving capabilities of schooling fish have been consistently observed in various formations, such as diamond, rectangular, phalanx, and in-line, as compared to an isolated swimmer [36]. Extensive investigations into the hydrodynamic performance of fish schools have examined diverse phase differences and amplitudes [33,40,46,47], further highlighting the significant energy benefits derived from different schooling formations.

However, it is important to note that the previous studies primarily focused on fish swimming in the same direction, i.e., in a schooling pattern. However, there is another commonly observed collective behavior pattern, the milling, believed to emerge during defensive or foraging activities. This specific

^{*}Corresponding author: zjudengjian@zju.edu.cn

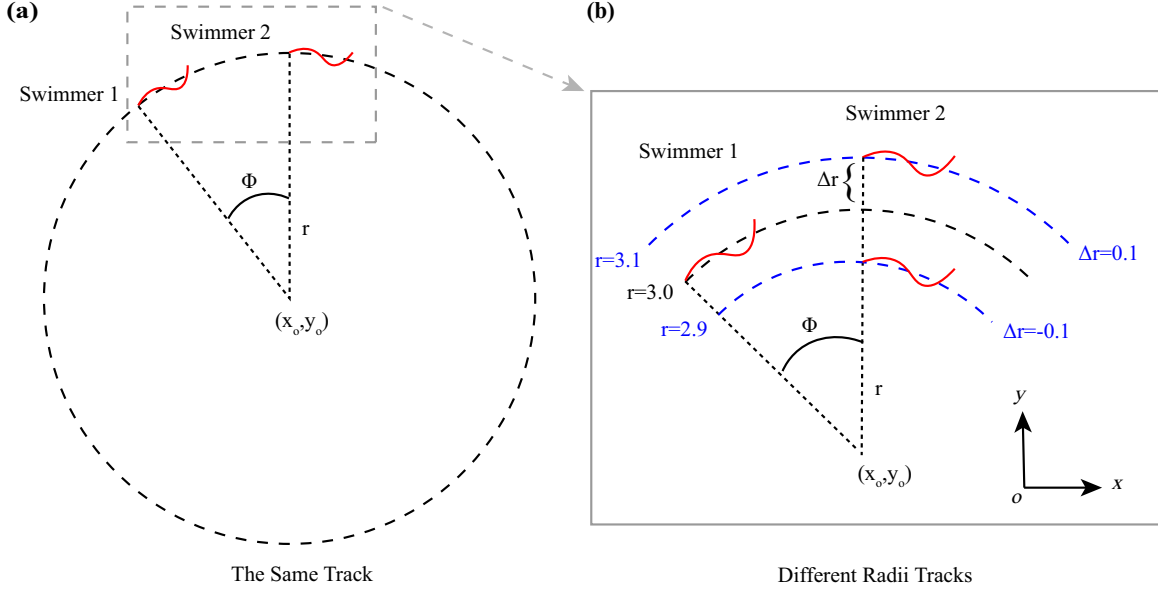


FIG. 1. (a) Schematic diagram illustrating two self-propelled swimmers swimming in the same track. The circumferential spacing between the swimmers is denoted as Φ in the form of an angle, which can be easily converted into the body length (BL). (b) Schematic diagram depicting concentric tracks with varying radii, where two swimmers are arranged in a leader-follower formation with a radial spacing denoted as Δr .

pattern offers unique dynamics, making it an intriguing subject for further investigation. Taking out an minimal element from this pattern, we propose a system consisting of two self-propelled swimmers equipped with control strategies for trajectory and velocity. This model allows us to delve into these open problems and gain a deeper understanding of the underlying mechanisms. Specifically, we investigate the dynamic interactions and energy benefits of these two swimmers that follow prescribed wavy motions, swimming in an initially quiescent fluid along circular tracks.

This paper is structured as follows. Section II presents the problem description, governing equations, PID approaches, and numerical validation. In Sec. III the detailed results about energy savings and efficiency gains are discussed. Finally, Sec. IV provides concluding remarks on the findings of this study.

II. NUMERICAL METHODOLOGY

We investigate the physical mechanisms that lead to energetically beneficial interactions between two self-propelled, identical swimmers in circular tracks. We consider two distinct scenarios, as shown in Fig. 1. The first scenario involves a pair of swimmers in a single track, with the follower able to make autonomous decisions to maintain a prescribed circumferential distance denoted by the angle Φ from the leader [see Fig. 1(a)]. In the second scenario, we study two swimmers swimming in two tracks with different radii, with a radial spacing between the tracks denoted by Δr [see Fig. 1(b)]. In both scenarios, the leader (or swimmer 1) always swims in the track with radius $r = 3.0$. Note that all lengths are normalized by the body length of the swimmers.

The self-propelled swimmers used in the simulations are modeled using two undulatory filaments of which the density distribution is based on a simplified physical model of

zebrafish, as described in Ref. [48], and a central pattern generator (CPG) controller, as described in Ref. [49]. The swimmers' motion consists of a rigid body motion and the undulation of the body. The former includes the translation of the mass center (or a reference point) and the rotation around it, while the latter represents the evolution of the swimmer's body curve. The rigid body motion is determined by the forces and torques exerted by the fluid on the swimmer's body, represented by

$$m\ddot{\mathbf{x}}_c = \mathbf{F}_c \quad (1)$$

and

$$I_z\ddot{\theta}_c = M_z. \quad (2)$$

Here m denotes the swimmer's mass, I_z represents the moment of inertia around the z axis, $\ddot{\mathbf{x}}_c$ is the acceleration of the reference point, $\ddot{\theta}_c$ is the angular acceleration, and \mathbf{F}_c and M_z denote the forces and torques exerted by the fluid on the swimmer, respectively. Undulations of the swimmer's body are generated by imposing a spatially and temporally varying body curvature, expressed as

$$k(s, t) = k_{base}(s, t) + k_{turn}(s, t), \quad (3)$$

where $k_{base}(s, t)$ is the curvature along the midline of the swimmer, which travels from the head to the tail as a wave, and $k_{turn}(s, t)$ represents the curvature of turning motion. This approach uses an arc-length coordinate system, as introduced in previous studies [25]. In the present study, the lateral displacement of the swimmer's midline is defined as the superimposition of two functions:

$$\zeta(s, t) = A(t)\tau(t)\sigma(s)\sin[2\pi s - \beta(t) + \Delta\varphi], \quad (4)$$

$$L(s, t) = B(t)\tau(t)s^p, \quad (5)$$

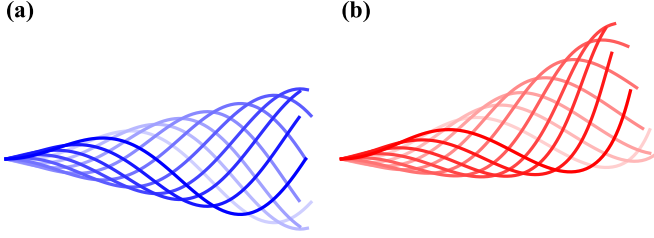


FIG. 2. Traced midlines from sequential instances in time (each separated by 0.1T and shown in lighter colors for earlier instances) are overlaid on top of one another to illustrate a typical whole undulatory cycle: (a) straight swimming and (b) turning swimming with offset.

where $\zeta(s, t)$ represents the prescribed backward traveling wave, and $L(s, t)$ is the offset function responsible for the swimmer's turning motion. The curvature of these functions can be obtained through numerical differentiation. We show the typical profiles for straight and turning swimming in Fig. 2. It is important to obtain the real midline curve of the swimmer by integrating the Frenet equations from the curvature, ensuring that the body length is inextensible [22].

In Eq. (4) the function $\sigma(s)$ represents the amplitude envelope of the traveling wave, where we have set $\sigma(s) = s$ to represent linear amplification from the head to the tail. The function $\tau(t)$ serves as the starting function, enabling the progressive application of the traveling curvature wave. Additionally, the function $\beta(t)$ regulates the frequency of tail beat and is defined as follows:

$$\beta(t) = \beta_0 + \int_0^t \beta' dt, \quad (6)$$

where the time-varying component $\beta'(t)$ is defined by the integral

$$\beta'(t) = \int_0^t -\gamma(\beta' - 2\pi\omega) dt, \quad (7)$$

Here the adjustable coefficient γ represents the transition rate from the current frequency of tail beat to its target value. In our study, we set ω as a constant and γ as 4. The phase difference, $\Delta\varphi$, can vary between different swimmers. The starting function, $\tau(t)$, is defined as

$$\tau(t) = \begin{cases} \frac{t}{T_s} - \frac{1}{2\pi} \sin\left(\frac{2\pi t}{T_s}\right) & 0 \leq t \leq T_s \\ 1.0 & t > T_s \end{cases}, \quad (8)$$

where T_s is the transition time of starting. In Eq. (5) the offset index is denoted by p , which is usually taken as $p = 2$ to indicate the quadratic. The two control parameters, $A(t)$ and $B(t)$, are tuned by a proportional-integral-derivative (PID) controller to ensure that the swimmer follows a target track with its target velocity.

The motion of a swimmer in a circular track is more complex than that moving in a straight line, especially when encountering the shedding wake of another swimmer. In order to maintain the swimmers in their specified tracks and maintain the desired spacing between them, a close-loop PID

control is employed. The errors are defined as

$$e_{dis} = r_{tar} - \sqrt{(x - x_o)^2 + (y - y_o)^2}, \quad (9)$$

$$e_{dir} = \theta_{tar} - \theta, \quad (10)$$

$$e_{vel} = V_{tar} - V, \quad (11)$$

where (x_o, y_o) denotes the coordinates of the track center, and r_{tar} is the target track radius; θ_{tar} represents the tangential direction of the swimmer's current position in the track, and θ is the swimmer's direction; V denotes the current swimming speed, and V_{tar} is its target value. The variables $A(t)$ and $B(t)$ are updated according to Eqs. (12)–(18) as

$$a'_{vel}(t) = c_1 e_{vel}(t) + c_2 \int_0^t e_{vel}(\tau) d\tau + c_3 \frac{de_{vel}(t)}{dt}, \quad (12)$$

$$b'_{dir}(t) = c_4 e_{dir}(t) + c_5 \int_0^t e_{dir}(\tau) d\tau + c_6 \frac{de_{dir}(t)}{dt}, \quad (13)$$

$$b'_{dis}(t) = c_7 e_{dis}(t) + c_8 \int_0^t e_{dis}(\tau) d\tau + c_9 \frac{de_{dis}(t)}{dt}, \quad (14)$$

$$a(t) = a_0 + \int_0^t a'_{vel}(\tau) d\tau, \quad (15)$$

$$b(t) = b_0 + \int_0^t [b'_{dir}(\tau) + b'_{dis}(\tau)] d\tau. \quad (16)$$

All variables denoted by a subscript 0 represent their initial values. The coefficients c_1 to c_9 in Eqs. (12) to (14) are fine-tuned to enhance the control performance of the PID controller. The control parameters described in Eqs. (4) and (5) are obtained using the following equations:

$$\delta A(t + \Delta t) = \delta A(t) + \Delta t \{ \alpha_A^2 [A(t) - a(t)] - 2\alpha_A \delta A(t) \}, \quad (17)$$

$$\delta B(t + \Delta t) = \delta B(t) + \Delta t \{ \alpha_B^2 [B(t) - b(t)] - 2\alpha_B \delta B(t) \}, \quad (18)$$

where α_A and α_B represent the coefficients of the smooth function. The control parameters are limited to the ranges of $A(t) \in [0.05, 0.25]$ and $B(t) \in [-0.2, 0.2]$ to ensure optimal performance [50–52].

The 2D incompressible Navier-Stokes equations serve as the governing equations for the flow in this study and are expressed as

$$\rho \left(\frac{\partial \mathbf{u}}{\partial t} + \mathbf{u} \cdot \nabla \mathbf{u} \right) = -\nabla p + \mu \nabla^2 \mathbf{u} + \mathbf{f}, \quad (19)$$

$$\nabla \cdot \mathbf{u} = 0, \quad (20)$$

where \mathbf{u} denotes the velocity, p represents the pressure, ρ is the fluid density, μ is the dynamic viscosity, and \mathbf{f} is the body force term. The latter represents the Eulerian momentum force on the surrounding fluid due to the immersed boundary, as constrained by the no-slip boundary condition. For details on the implementation of these equations, readers can refer to our previous work [49,53].

In order to evaluate the swimming efficiency, we use the cost of transport (CoT) metric, defined as

$$\text{CoT} = \frac{\bar{P}}{U}, \quad (21)$$

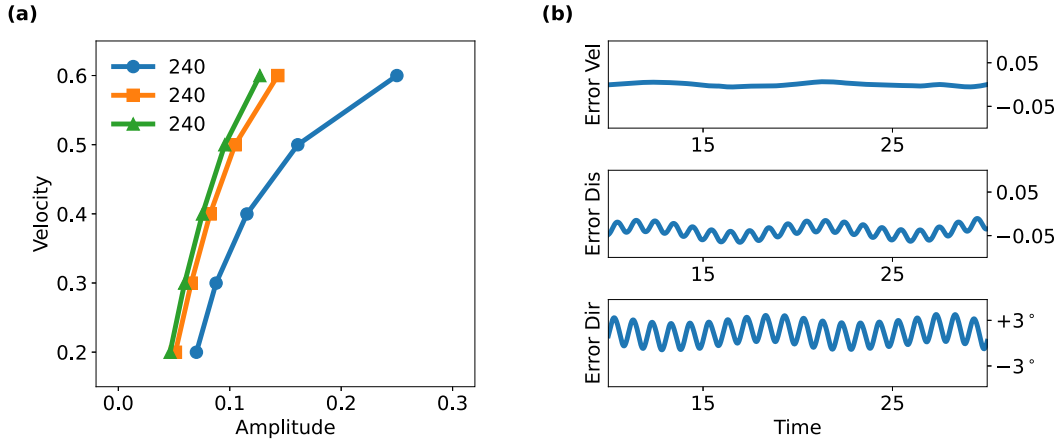


FIG. 3. (a) Grid-independence analysis: A simulation of a solitary swimmer swimming at a steady velocity controlled by PID is conducted to test grid independence and PID stability. The PID coefficients used in this case are the same as those used for the two swimmers. (b) Stability of trajectory under PID control for a solitary swimmer swimming in a circular track is shown by the motion indicator. The indicator is the error between the current value and the control target value, which is defined in Eqs. (9)–(11).

where \bar{P} represents the total motion power consumed by swimming at an averaged speed of U [54]. The CoT serves as a measure of the energy consumption of a swimmer per unit distance. In the case of a given swimmer, minimizing the CoT metric is equivalent to minimizing fuel consumption. The swimming efficiency of a swimmer is inversely proportional to its CoT value, meaning that a higher swimming efficiency leads to a lower CoT value and vice versa. The instantaneous power P is calculated by

$$P = \int -\mathbf{F}(s, t) \mathbf{U}(s, t) ds, \quad (22)$$

where ds is the length of a differential element along the body, $-\mathbf{F}(s, t)$ represents the force exerted by the swimmer on the surrounding fluid, and $\mathbf{U}(s, t)$ represents the velocity of this element. Then the averaged power is obtained by integrating over a certain period, as

$$\bar{P} = \frac{1}{T} \int_{t-T}^t P dt. \quad (23)$$

To validate the present numerical method and PID approach, the case of a single self-propelled swimmer on a circular track is simulated. The accuracy of the trajectory is evaluated by the errors of distance and direction, which show fluctuations of less than 0.1 and 6° , respectively, as depicted in Fig. 3(b). The steadiness of the velocity is evaluated by the error of velocity, which remains less than 2% after the ramped-up process. We also investigate the grid independence of their method by examining the steady velocity of the single swimmer obtained from different grid resolutions. We find that the grid = 160 is sufficient to achieve accurate results, with a discrepancy of corresponding amplitude of less than 5%, as shown in Fig. 3(a). The present numerical method has also been validated and applied to various other problems, including the fluid dynamics induced by a circular cylinder with flexible filaments and the unsteady flow around two flexible filaments in a tandem arrangement [53,55]. To validate the model, we also test on two in-line swimmers, with a separating distance of 1 BL (body length). Figure 4 shows the energy

consumption of the two swimmers. The leader's energy consumption remains at a stable level, while the follower's energy consumption exhibits a sinusoidal-like variation as the phase difference between them changes. Within a certain range of phase differences, the follower gets energy benefits. These results align with previous research [56].

III. RESULTS

We present the simulated results for the studies of varying circumferential spacing (Φ) and radial spacing (Δr), corresponding to the two different scenarios illustrated in Fig. 1. In both, the phase difference $\Delta\phi$ between the two swimmers is the key factor to achieve optimal energetic benefits. A simulation for a solitary swimmer is also carried out to provide a basis for comparison. Before proceeding to the two scenarios, we present in Fig. 5 the flow patterns of this two-swimmer system, with their detailed discussion given in the following sections.

A. Circumferential spacing

First, we consider a scenario where two swimmers maintain a constant circumferential spacing denoted by Φ while

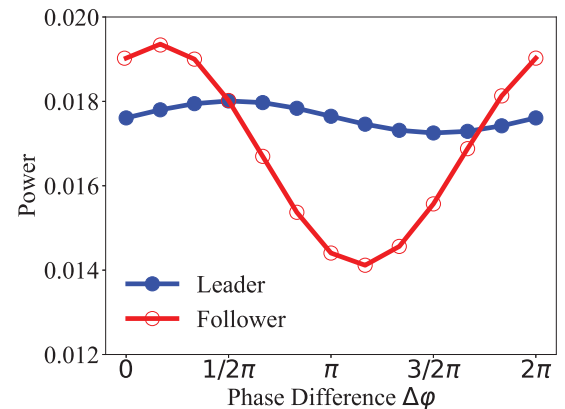


FIG. 4. Energy consumption of two in-line swimmers.

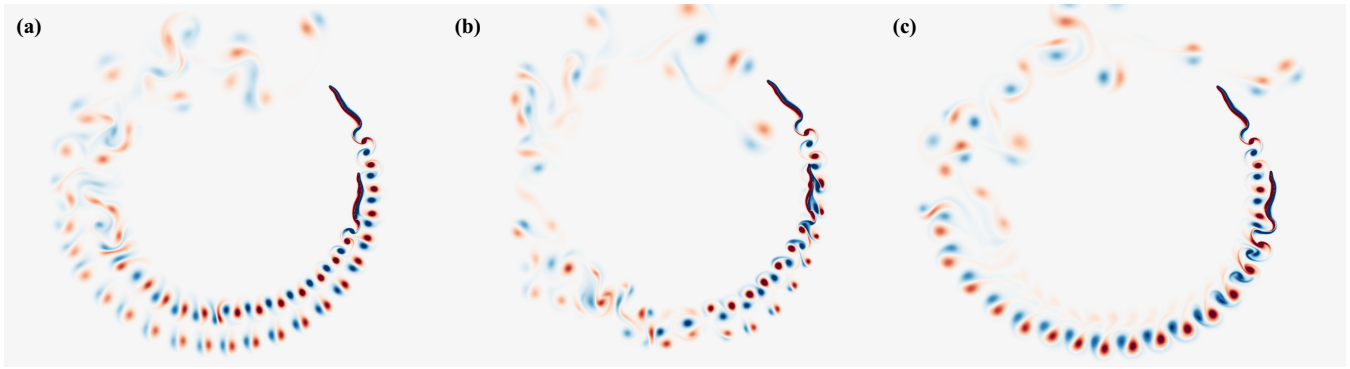


FIG. 5. Vorticity contours of three different radii cases at the same instant $t/T = 30$: (a) the inner follower case with $\Delta r = -0.3$; (b) the same track case with $\Delta r = 0$; and (c) the outer follower case with $\Delta r = 0.3$. The range of the vorticity contours is from -5.0 (blue or dark gray) to 5.0 (red or light gray).

swimming in a predefined circular track. With the aid of a direction controller, the leader and follower are able to swim persistently and steadily along the same track, with any lateral deviation effect being weak and negligible. In the current PID approach, the swimmers adjust their direction and velocity using an offset function and amplitude, respectively, which eventually leads to their desired motion. It is noteworthy that both swimmers utilize identical coefficients in the PID approach, but due to the difference in the surrounding flow fields, they adjust $A(t)$ and $B(t)$ to swim appropriately.

We present a case study that demonstrates the performance of the PID controller in achieving energy savings. Figure 6 illustrates the discrepancy of directions. Additionally, a velocity controller is employed to maintain a stable circumferential spacing Φ , forming the basis for studying the

circumferential effect. The variation of spacing Φ is depicted in Fig. 6(a), while Figs. 6(c) and 6(d) display the variation of $A(t)$ and $B(t)$ of the leader and the follower, respectively. The follower exhibits a smaller $A(t)$ than the leader, indicating that it can maintain the same velocity with a smaller amplitude, leading to improved swimming efficiency. Furthermore, the $B(t)$ of the follower is also smaller than that of the leader, suggesting that it can adjust direction with less action. The follower leverages the vortex in the wake of the leader, which reduces the offset and facilitates effortless turning. This behavior also contributes to improving swimming efficiency, which is not possible to be observed in straight-motion cases.

We examine the impact of various phase differences $\Delta\varphi$ between the undulating motions of two swimmers on a constant circumferential spacing. Due to the generation of vortex structures resulting from the unsteady motions of the leader, a discernible difference in performance is observed between the leader and the follower. The power cost of the leader remains stable regardless of the phase difference, being almost indistinguishable from that of a solitary swimmer (Fig. 7). In contrast, the power consumption of the follower is significantly affected by the phase difference. The relationship between power costs and phase difference is approximately sinusoidal, consistent with the findings of the previous research [56]. Notably, the optimal and worst phases differ by π . Even at the worst phase, the follower exhibits an energy advantage over a solitary swimmer. The optimal phase shift for different Φ and shift speeds is approximately $\pi/\Delta\Phi$ (based on the BL). Comprehensive details and insights can be found in Fig. 8.

To further investigate the circumferential effect, we conduct a series of simulations at different phase differences $\Delta\varphi$. The range of circumferential spacing Φ spans from 30° to 50° , which can be converted into a distance of 0.6 – 1.6 BL from the tail of the leader to the head of the follower. Figure 8 displays a map comprising circumferential spacing Φ and phase difference $\Delta\varphi$, with data duplicated twice along the phase difference axis to clearly demonstrate the periodic pattern. As Φ decreases, the vortices encountered by the follower tend to be stronger, resulting in increased energy consumption by the follower to maintain formation. In some cases, it becomes challenging to sustain the same circular track when Φ is less than 30° (0.6 BL). On the other hand, if Φ exceeds 50° (1.6 BL), the hydrodynamic advantage induced by the leader

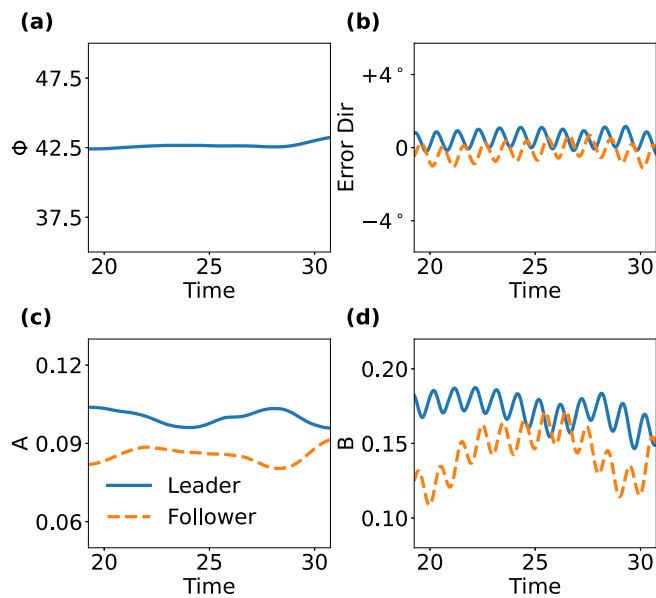


FIG. 6. (a) Circumferential spacing Φ as a function of time for the case where $\Phi = 42.5^\circ$ and $\Delta\varphi = \frac{2}{3}\pi$. (b) Directional error between the swimming direction θ and the tangential direction θ_{tar} of the current position in the track. (c) Variation of the amplitude $A(t)$ for both the leader and the follower with time. (d) Variation of the offset $B(t)$ for both the leader and the follower with time.

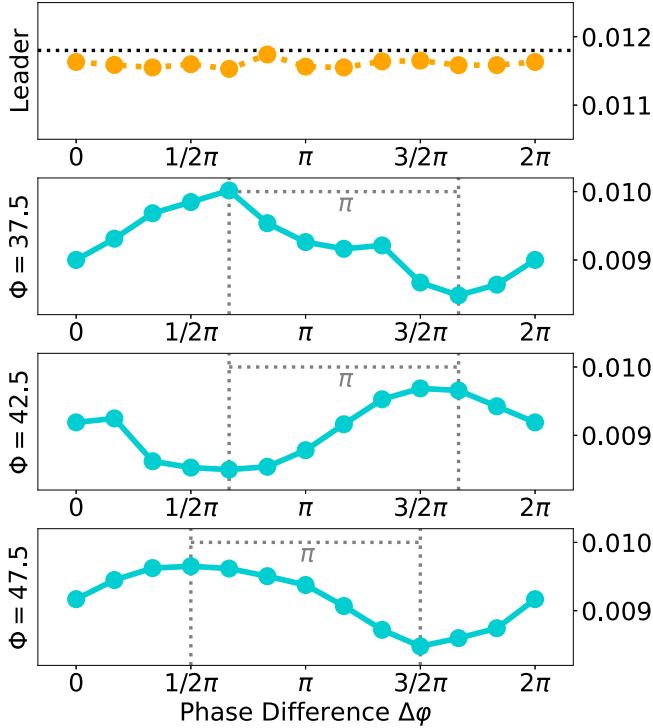


FIG. 7. Power costs shown as a function of the phase difference $\Delta\phi$ for the leader, and the follower with the spacing of $\Phi = 37.5^\circ$, 42.5° , and 47.5° (from top to bottom). The black dashed line in the top panel marks the power cost of a solitary swimmer, as a baseline for comparison. Note that the power cost of the leader is shown only for $\Phi = 37.5^\circ$, which varies little among different values of spacing.

appears to be weak and negligible with increasing spacing. Within the current parametric space, the optimal Φ is found to be 42.5° (1.2 BL), wherein a wider range of phase differences ($\frac{1}{3}\pi - \frac{5}{6}\pi$) can provide satisfactory efficiency gains, as indicated by a wider dark band in Fig. 8. Generally, the optimal phase difference is found to be linearly correlated with circumferential spacing Φ within the scope of this study. This behavior is similar to the vortex phase matching observed in prior research, indicating that for small Φ , the wake influence of the leader on the follower characterizing as the ability of the follower exploiting the vortices in the wake, exhibits insignificant differences with straight-motion cases.

B. Radial spacing

We position two swimmers in different tracks that are concentric with varying radii. The difference in radii staggers the leader and follower by a lateral distance, allowing for the lateral effect of wake vortex to be taken into account. The leader swims in the middle track, followed by the follower with constant radial and circumferential spacing. The results of the follower in different tracks are plotted in Fig. 9. To maintain the formation, the follower’s velocity in the tracks with different radii shows a clear difference. When the radius of the inner track decreases, the follower’s velocity compared to that of the leader decreases accordingly, and vice versa. However, due to the influence of hydrodynamic interaction,

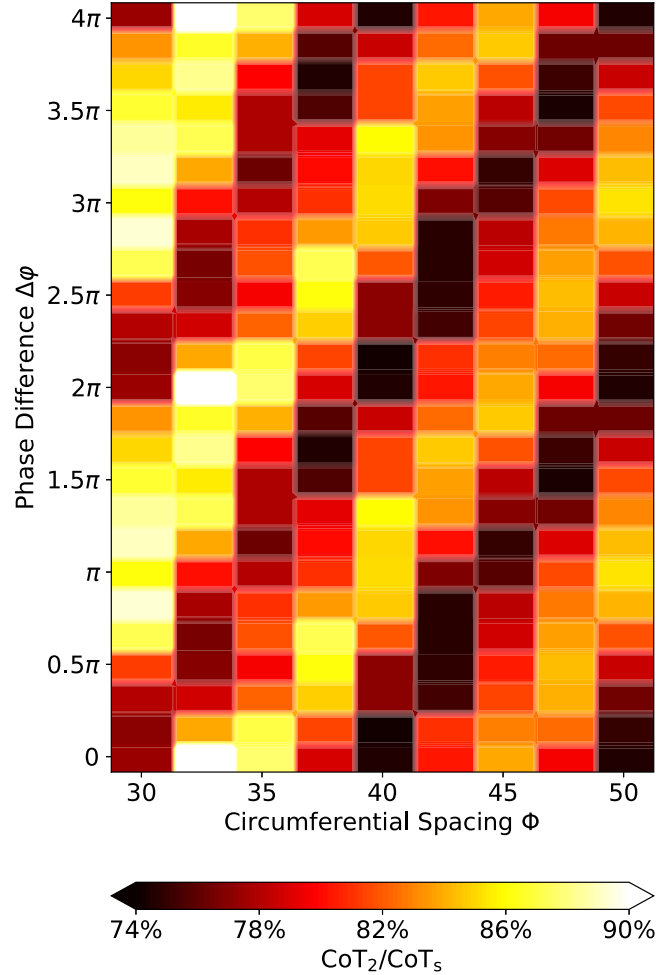


FIG. 8. The coefficient of thrust efficiency (CoT) shown as a function of the phase difference and the circumferential spacing Φ , normalized by that of a solitary swimmer. The data are duplicated twice along the phase difference axis to more clearly demonstrate the periodic pattern.

the power cost does not vary linearly with velocity. The lowest power cost, corresponding to the highest efficiency, occurs when $\Delta r = 0$, resulting in a nearly 26% reduction in power cost compared to a solitary swimmer. As the track lies in the inner position, the follower gradually moves away from the wake vortex’s moving path, resulting in weakened hydrodynamic interaction. Although the follower’s velocity is slower, the power cost saving can reach only about 10% in the three inner tracks. For the three outer tracks, the influence of phase difference is more apparent and determines whether the follower’s power cost is saving or consumptive. It is indicated that the phase match is more critical for individuals in the outer position of the milling pattern. The optimal phase difference allows the faster follower in outer tracks to incur almost the same power cost as the inner leader, while phase mismatch makes maintaining the formation more challenging.

Utilizing the methodology outlined in the previous section, wherein the data are duplicated twice, we generate a map, as presented in Fig. 10. The map is composed of the radial spacing Δr and the phase difference $\Delta\phi$ and is designed to provide

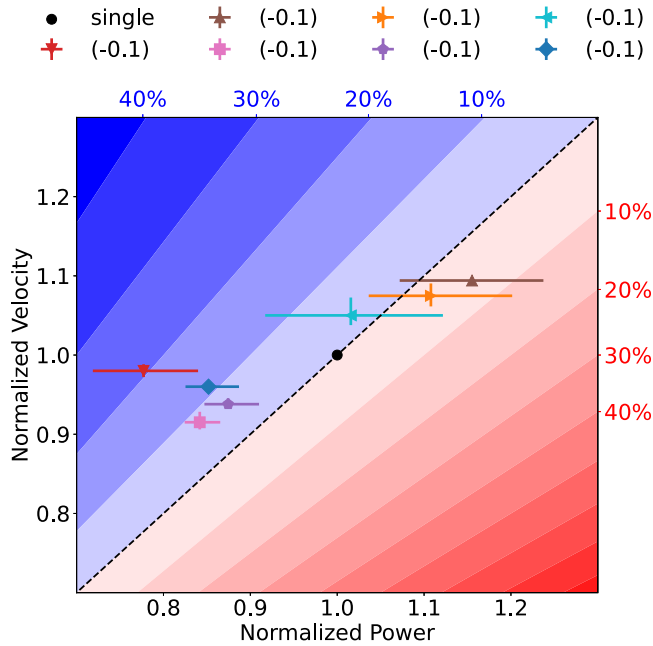


FIG. 9. Scatter plot showing the velocity and power of the follower in different radii tracks, normalized by the data of a solitary swimmer. The symbols represent the average velocity and corresponding power at a certain radial spacing Δr . The horizontal lines denote the range of power in different phase difference cases, and the vertical lines denote the range of velocity. The solid dot represents the solitary swimmer, and the dashed line is the isoline of its efficiency. In the background, blue (dark gray, representing savings) and red (light gray, representing consumption) are used to clearly demonstrate the efficiency of each case.

a more detailed representation of cases with various phase differences. A diverging colormap is adopted to distinguish between energy saving and consumptive states, with blue representing saving and red denoting consumptive states. Our findings indicate that the hydrodynamic interaction is positive for all inner followers. However, the available vortices become weaker and the energy savings tend to decrease as the radial spacing Δr decreases. The most efficient case occurs when $\Delta r = 0$, signifying that the follower in the same track can take full advantage of the wake vortices. Conversely, the radial difference weakens the exploitation of the wake vortex.

The cases involving an outer follower are more complex. As illustrated in the contour, since the wake vortices of the leader move backward and outward in terms of radial direction, the outer follower tends to encounter a stronger vortex, implying a more difficult exploitation and a more laborious swimming. Therefore, the more laborious cases predominate when the radial spacing Δr increases. For $\Delta r = 0.1$, half of the cases exhibit saving and consumptive states. The phase match achieves about 14% energy saving, while the phase mismatch causes less than 5% loss. This indicates that for an outer follower, it is beneficial to keep the inside peer closer than 0.1 BL and maintain the phase match.

To gain a more comprehensive understanding of the impact of the phase difference $\Delta\phi$ on efficiency, a statistical analysis is conducted for all efficiency data in the form of a

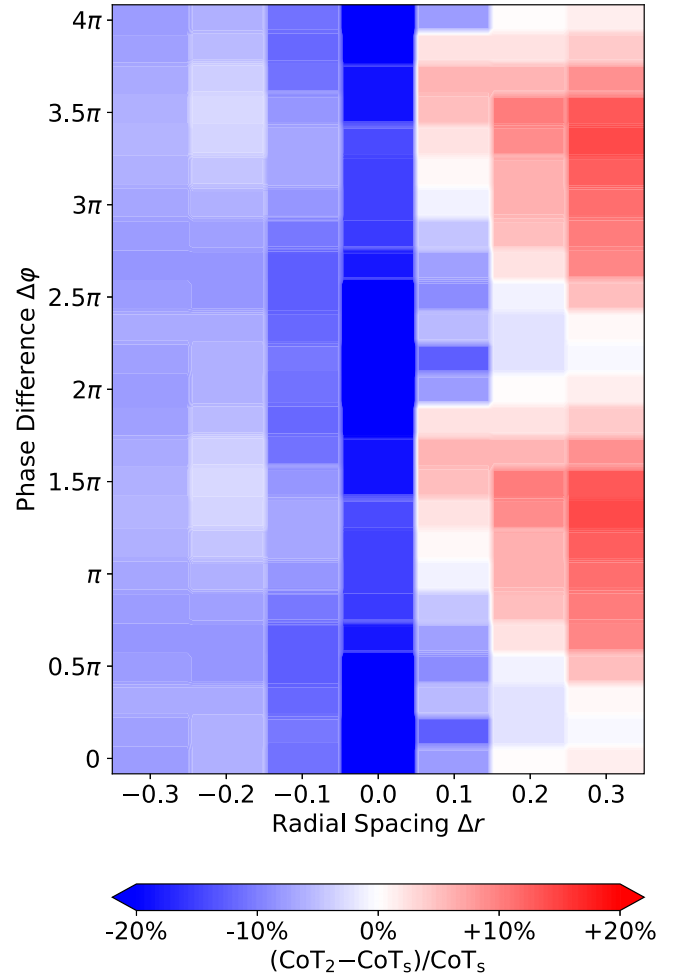


FIG. 10. Coefficient of thrust efficiency (CoT), shown as a function of the phase difference and the radial spacing Δr , normalized by that of a solitary swimmer. A diverging colormap (blue-white-red or dark gray to light gray) has been adopted to distinguish between savings and consumption more conveniently.

box plot (Fig. 11). The plot demonstrates a V-shaped trend in efficiency, where the lowest box represents the most efficient cases in which $\Delta r = 0$. The black dashed line represents the efficiency of a solitary swimmer in the middle track. The brown crosses represent those in different radii tracks. In comparison to the outer cases, where the efficiencies vary in relation to the phase difference and traverse that of a solitary swimmer, the efficiencies of the inner cases demonstrate only slight variation. As the radial spacing Δr decreases, the efficiency of the inner follower becomes nearly constant with respect to the phase difference $\Delta\phi$. This is primarily due to the weaker impact exerted by the outward moving wake vortices induced by the leader on the inner follower, as the radial spacing Δr decreases. Although the energy savings obtained are not as significant as those resulting from direct vortices exploitation, the inner follower can still obtain a certain level of energetic benefit, approximately 8%, regardless of the phase difference, when an outer leader swims in front of it.

Compared to the cases of a solitary swimmer in the different radii tracks, we find that the energetic benefit of inner

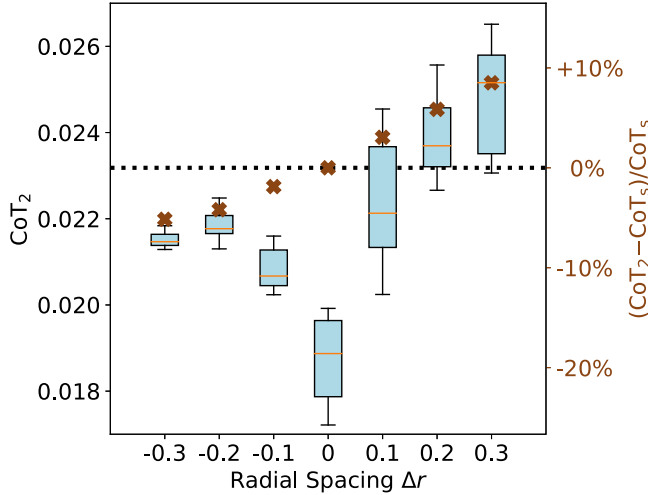


FIG. 11. Box plot of the coefficient of thrust efficiency (CoT) for the follower in different radii tracks, with the black dashed line denoting the CoT efficiency of a solitary swimmer in the middle track and the brown crosses denoting those in different radii tracks.

follower comes from both the hydrodynamic interaction and the lower velocity corresponding to the smaller CoT . For the outer follower, in spite of the higher velocity corresponding to the higher CoT , it is clear that the hydrodynamic interaction could be constructive or destructive, which depends on the phase difference.

Figure 5 showcases the vorticity contours for three different radii configurations at the same instant ($t/T = 30$) and a fixed phase difference ($\Delta\varphi = \frac{4}{3}\pi$). As a swimmer follows a circular track, the wake vortices form an arc and exhibit a tendency to radially expand outward. Due to the variation in radii between the inner and outer tracks, the leader and follower experience a discrepancy in their velocities while maintaining the formation. Consequently, despite having the same shedding frequency, the spacing between the wake vortices differs. This outward expansion of vortices leads to a more pronounced impact on the outer side follower compared to the inner side one.

The variation in swimming speed between two swimmers in different formations results in different energy gains during their cooperative swimming, which is evident in the characteristics of the wake vortices—whether they remain separate, break up, or merge. In the case of $\Delta r = -0.3$, representing an inner follower, two distinct strings of wake vortices can be observed, as shown in Fig. 5(a). These wake vortices shed, move, and dissipate without direct contact between the leader and follower. The influence of the leader on the inner follower is relatively weak and indirect compared to other cases. Since the vortices are not entangled, the impact of the phase difference $\Delta\varphi$ between the two swimmers is relatively small.

For $\Delta r = 0$, the follower continues to pass through the wake vortices induced by the leader. The vortex pair encountered by a follower is stretched along the swimmer's motion direction, as shown in Fig. 5(b). The results indicate that the negative (blue) vortex has a more distinct deformation and decays faster than the positive one (red). With the flapping motion of the tail, the follower sheds a new vortex

pair, which tends to entangle the stretched pair. Most of the negative vortices merge with the new vortex pair, while the positive vortices tend to decay rapidly. The wake vortices of the leader retain only a string of weaker vortex pairs. The merging process strengthens the wake vortices of the follower and causes the vortex pair to rotate clockwise. The follower passes through the wake vortices of the leader directly and breaks them up, resulting in a significant energy gain affected by the phase difference matching.

For $\Delta r = 0.3$, the wake vortices of the inner leader move outward radially, approaching closer to the outer follower and its wake vortices, as shown in Fig. 5(c). When the two swimmers are in the appropriate phase, their wake vortices tend to merge, resulting in the formation of a strong vortex pair. At the initial stage when the leader sheds the wake vortices, it is difficult for the outer follower to contact with the inner wake vortices due to the radii difference in the tracks. The wake vortices of the inner leader remain almost intact until they are merged with the outer vortices. In this case, the energy loss of the inner vortex is small, and it is challenging to gain high energy for the outer follower.

IV. CONCLUSIONS

In this paper we present a demonstration of the energetic advantages of coordinated swimming for two swimmers in circular tracks through a series of simulations. First, a leader-follower formation in the same track, corresponding to the circumferential effect, is examined to investigate energy savings. It is observed that there exists an approximately sinusoidal relationship between the power cost and the phase difference $\Delta\varphi$. The optimal phase difference is linearly correlated to the circumferential spacing Φ , which is similar to the cases of straight motion in previous studies. It is believed that two factors contribute to the energy saving, namely, the ability to achieve the same velocity with a smaller amplitude, and the ability to achieve the same turning with a smaller action. The latter is not apparent in previous studies involving straight motion.

In addition, we investigate the radial effect, which characterizes the scenario where the leader and follower swim on different radii tracks. For the inner follower, the influence of hydrodynamic interaction becomes weaker with a decreasing radial spacing Δr , while there is always a certain energetic benefit (8%) regardless of the phase difference $\Delta\varphi$. For the outer follower, the energetic benefit and consumption coexist when the radial spacing is small ($\Delta r \leq 0.1$), depending on the phase difference $\Delta\varphi$. As the radial spacing becomes larger, the energetic consumption tends to become more dominant. The follower swimming in the same track ($\Delta r = 0$) can take full advantage of the wake vortices and obtain the most energetic benefit (-26%).

In terms of the energetic benefit, both swimmers moving in the same track, similar to the straight-motion cases, can be highly efficient. For a school of milling pattern, the individuals on the inside can easily obtain the energetic benefits, while the outside ones have to stay close enough to the inner one with a proper phase difference to gain energetic benefits. We observe that swimming for the follower tends to be more laborious

(up to 16%) when the radial spacing becomes larger or is in a mismatched phase.

We believe that two-dimensional simulations and low-order models are essential before completely exploring related problems in three-dimensional flow. Furthermore, we anticipate the possibility of applying a more effective and accurate control method in a larger school of swimmers. The findings and highlights of this work are relevant to the design of

multiple robotic swimmers, which requires a full understanding of the involved hydrodynamic characteristics to achieve satisfactory efficiency and collective cooperation.

ACKNOWLEDGMENT

This research has been supported by the National Natural Science Foundation of China (Grant No. 92252102).

-
- [1] J. Lazarus, The early warning function of flocking in birds: An experimental study with captive quelea, *Anim. Behav.* **27**, 855 (1979).
- [2] L. Landeau and J. Terborgh, Oddity and the ‘confusion effect’ in predation, *Anim. Behav.* **34**, 1372 (1986).
- [3] P. Romanczuk, I. D. Couzin, and L. Schimansky-Geier, Collective motion due to individual escape and pursuit response, *Phys. Rev. Lett.* **102**, 010602 (2009).
- [4] R. Bastien and P. Romanczuk, A model of collective behavior based purely on vision, *Sci. Adv.* **6**, eaay0792 (2020).
- [5] J. R. Krebs, M. H. MacRoberts, and J. Cullen, Flocking and feeding in the great tit *Parus major*—An experimental study, *Ibis* **114**, 507 (1972).
- [6] T. Pitcher, A. Magurran, and I. Winfield, Fish in larger shoals find food faster, *Behav. Ecol. Sociobiol.* **10**, 149 (1982).
- [7] K. S. Norris and C. R. Schilt, Cooperative societies in three-dimensional space: On the origins of aggregations, flocks, and schools, with special reference to dolphins and fish, *Ethol. Sociobiol.* **9**, 149 (1988).
- [8] C. C. Ioannou, V. Guttal, and I. D. Couzin, Predatory fish select for coordinated collective motion in virtual prey, *Science* **337**, 1212 (2012).
- [9] V. E. Brock and R. H. Riffenburgh, Fish schooling: A possible factor in reducing predation, *ICES J. Mar. Sci.* **25**, 307 (1960).
- [10] D. Cushing and F. H. Jones, Why do fish school? *Nature (London)* **218**, 918 (1968).
- [11] J. Deng and D. Liu, Spontaneous response of a self-organized fish school to a predator, *Bioinspir. Biomim.* **16**, 046013 (2021).
- [12] D. Weihs, Hydromechanics of fish schooling, *Nature (London)* **241**, 290 (1973).
- [13] D. G. Harper and R. W. Blake, Fast-start performance of rainbow trout *Salmo gairdneri* and northern pike *Esox lucius*, *J. Exp. Biol.* **150**, 321 (1990).
- [14] V. van Ginneken, E. Antonissen, U. K. Muller, R. Booms, E. Eding, J. Verreth, and G. van den Thillart, Eel migration to the Sargasso: Remarkably high swimming efficiency and low energy costs, *J. Exp. Biol.* **208**, 1329 (2005).
- [15] C. Breder, Vortices and fish schools, *Zoologica* **50**, 97 (1965).
- [16] S. Neill and J. M. Cullen, Experiments on whether schooling by their prey affects the hunting behaviour of cephalopods and fish predators, *J. Zool.* **172**, 549 (1974).
- [17] P. F. Major, Predator-prey interactions in two schooling fishes, *Caranx ignobilis* and *Stolephorus purpureus*, *Anim. Behav.* **26**, 760 (1978).
- [18] J. Herskin and J. Steffensen, Energy savings in sea bass swimming in a school: Measurements of tail beat frequency and oxygen consumption at different swimming speeds, *J. Fish Biol.* **53**, 366 (1998).
- [19] V. Belyayev and G. Zuyev, Hydrodynamic hypothesis of school formation in fishes, *Prob. Ichthyol.* **9**, 578 (1969).
- [20] H.-B. Deng, Y.-Q. Xu, D.-D. Chen, H. Dai, J. Wu, and F.-B. Tian, On numerical modeling of animal swimming and flight, *Comput. Mech.* **52**, 1221 (2013).
- [21] J. Carling, T. L. Williams, and G. Bowtell, Self-propelled anguilliform swimming: Simultaneous solution of the two-dimensional Navier-Stokes equations and Newton’s laws of motion, *J. Exp. Biol.* **201**, 3143 (1998).
- [22] S. Kern and P. Koumoutsakos, Simulations of optimized anguilliform swimming, *J. Exp. Biol.* **209**, 4841 (2006).
- [23] I. Borazjani and F. Sotiropoulos, Numerical investigation of the hydrodynamics of carangiform swimming in the transitional and inertial flow regimes, *J. Exp. Biol.* **211**, 1541 (2008).
- [24] A. A. Shirgaonkar, M. A. MacIver, and N. A. Patankar, A new mathematical formulation and fast algorithm for fully resolved simulation of self-propulsion, *J. Comput. Phys.* **228**, 2366 (2009).
- [25] G. Liu, Y.-L. Yu, and B.-G. Tong, Flow control by means of a traveling curvature wave in fishlike escape responses, *Phys. Rev. E* **84**, 056312 (2011).
- [26] M. Bergmann, A. Iollo, and R. Mittal, Effect of caudal fin flexibility on the propulsive efficiency of a fish-like swimmer, *Bioinspir. Biomim.* **9**, 046001 (2014).
- [27] D. A. P. Reid, H. Hildenbrandt, J. T. Padding, and C. K. Hemelrijk, Fluid dynamics of moving fish in a two-dimensional multiparticle collision dynamics model, *Phys. Rev. E* **85**, 021901 (2012).
- [28] J. D. Eldredge, Numerical simulations of undulatory swimming at moderate Reynolds number, *Bioinspir. Biomim.* **1**, S19 (2006).
- [29] G. Tokić and D. K. Yue, Optimal shape and motion of undulatory swimming organisms, *Proc. R. Soc. B* **279**, 3065 (2012).
- [30] C. Eloy, On the best design for undulatory swimming, *J. Fluid Mech.* **717**, 48 (2013).
- [31] W. M. Van Rees, M. Gazzola, and P. Koumoutsakos, Optimal shapes for anguilliform swimmers at intermediate Reynolds numbers, *J. Fluid Mech.* **722**, R3 (2013).
- [32] J. C. Liao, D. N. Beal, G. V. Lauder, and M. S. Triantafyllou, Fish exploiting vortices decrease muscle activity, *Science* **302**, 1566 (2003).
- [33] J. Deng, X.-M. Shao, and Z.-S. Yu, Hydrodynamic studies on two traveling wavy foils in tandem arrangement, *Phys. Fluids* **19**, 113104 (2007).
- [34] P. A. Dewey, D. B. Quinn, B. M. Boschitsch, and A. J. Smits, Propulsive performance of unsteady tandem hydrofoils in a side-by-side configuration, *Phys. Fluids* **26**, 041903 (2014).

- [35] S.-Y. Chen, Y.-H. J. Fei, Y.-C. Chen, K.-J. Chi, and J.-T. Yang, The swimming patterns and energy-saving mechanism revealed from three fish in a school, *Ocean Eng.* **122**, 22 (2016).
- [36] C. Hemelrijk, D. Reid, H. Hildenbrandt, and J. Padding, The increased efficiency of fish swimming in a school, *Fish Fish.* **16**, 511 (2015).
- [37] V. Raspa, R. Godoy-Diana, and B. Thiria, Topology-induced effect in biomimetic propulsive wakes, *J. Fluid Mech.* **729**, 377 (2013).
- [38] M. S. U. Khalid, I. Akhtar, and H. Dong, Hydrodynamics of a tandem fish school with asynchronous undulation of individuals, *J. Fluids Struct.* **66**, 19 (2016).
- [39] G. Xu, W. Duan, and W. Xu, The propulsion of two flapping foils with tandem configuration and vortex interactions, *Phys. Fluids* **29**, 097102 (2017).
- [40] G.-J. Dong and X.-Y. Lu, Characteristics of flow over traveling wavy foils in a side-by-side arrangement, *Phys. Fluids* **19**, 057107 (2007).
- [41] E. Kanso and P. Newton, Locomotory advantages to flapping out of phase, *Exp. Mech.* **50**, 1367 (2010).
- [42] Z.-R. Peng, H. Huang, and X.-Y. Lu, Collective locomotion of two closely spaced self-propelled flapping plates, *J. Fluid Mech.* **849**, 1068 (2018).
- [43] B. M. Boschitsch, P. A. Dewey, and A. J. Smits, Propulsive performance of unsteady tandem hydrofoils in an in-line configuration, *Phys. Fluids* **26**, 051901 (2014).
- [44] R. Godoy-Diana, J. Vacher, V. Raspa, and B. Thiria, On the fluid dynamical effects of synchronization in side-by-side swimmers, *Biomimetics* **4**, 77 (2019).
- [45] Y. Bao, D. Zhou, J. Tao, Z. Peng, H. Zhu, Z. Sun, and H. Tong, Dynamic interference of two anti-phase flapping foils in side-by-side arrangement in an incompressible flow, *Phys. Fluids* **29**, 033601 (2017).
- [46] X. Lin, J. Wu, T. Zhang, and L. Yang, Phase difference effect on collective locomotion of two tandem autopropelled flapping foils, *Phys. Rev. Fluids* **4**, 054101 (2019).
- [47] J. W. Newbolt, J. Zhang, and L. Ristroph, Flow interactions between uncoordinated flapping swimmers give rise to group cohesion, *Proc. Natl. Acad. Sci. USA* **116**, 2419 (2019).
- [48] M. Gazzola, P. Chatelain, W. M. Van Rees, and P. Koumoutsakos, Simulations of single and multiple swimmers with non-divergence free deforming geometries, *J. Comput. Phys.* **230**, 7093 (2011).
- [49] L. Li, D. Liu, J. Deng, M. J. Lutz, and G. Xie, Fish can save energy via proprioceptive sensing, *Bioinspir. Biomim.* **16**, 056013 (2021).
- [50] R. Bale, A. A. Shirgaonkar, I. D. Neveln, A. P. S. Bhalla, M. A. MacIver, and N. A. Patankar, Separability of drag and thrust in undulatory animals and machines, *Sci. Rep.* **4**, 7329 (2014).
- [51] S. P. Howe and H. C. Astley, The control of routine fish maneuvers: Connecting midline kinematics to turn outcomes, *J. Exp. Zool. A* **333**, 579 (2020).
- [52] G. Li, H. Liu, U. K. Müller, C. J. Voesenek, and J. L. Van Leeuwen, Fishes regulate tail-beat kinematics to minimize speed-specific cost of transport, *Proc. R. Soc. B* **288**, 20211601 (2021).
- [53] J. Deng, X. Mao, and F. Xie, Dynamics of two-dimensional flow around a circular cylinder with flexible filaments attached, *Phys. Rev. E* **100**, 053107 (2019).
- [54] J. L. Kendall, K. S. Lucey, E. A. Jones, J. Wang, and D. J. Ellerby, Mechanical and energetic factors underlying gait transitions in bluegill sunfish (*Lepomis macrochirus*), *J. Exp. Biol.* **210**, 4265 (2007).
- [55] F. Xie and J. Deng, A further study of inverted hydrodynamic drafting for flow past two flexible filaments in tandem arrangement, *Prog. Comput. Fluid Dyn.* **18**, 164 (2018).
- [56] L. Li, M. Nagy, J. M. Graving, J. Bak-Coleman, G. Xie, and I. D. Couzin, Vortex phase matching as a strategy for schooling in robots and in fish, *Nat. Commun.* **11**, 5408 (2020).